

Flow boiling CHF in microgravity

Hui Zhang^a, Issam Mudawar^{a,*}, Mohammad M. Hasan^b

^a *Boiling and Two-phase Flow Laboratory, School of Mechanical Engineering, Purdue University, 1288 Mechanical Engineering Building, West Lafayette, IN 47907, USA*

^b *NASA Glenn Research Center, 21000 Brookpark Road, Cleveland, OH 44135, USA*

Received 15 October 2004; received in revised form 5 February 2005

Available online 18 April 2005

Abstract

Poor understanding of flow boiling in microgravity has recently emerged as a key obstacle to the development of many types of power generation and life support systems intended for space exploration. This study examines flow boiling CHF in microgravity that was achieved in parabolic flight experiments with FC-72 onboard NASA's KC-135 turbopump. At high heat fluxes, bubbles quickly coalesced into fairly large vapor patches along the heated wall. As CHF was approached, these patches grew in length and formed a wavy vapor layer that propagated along the wall, permitting liquid access only in the wave troughs. CHF was triggered by separation of the liquid–vapor interface from the wall due to intense vapor effusion in the troughs. This behavior is consistent with, and accurately predicted by the Interfacial Lift-off CHF Model. It is shown that at low velocities CHF in microgravity is significantly smaller than in horizontal flow on earth. CHF differences between the two environments decreased with increasing velocity, culminating in virtual convergence at about 1.5 m/s. This proves it is possible to design inertia-dominated systems by maintaining flow velocities above the convergence limit. Such systems allow data, correlations, and/or models developed on earth to be safely implemented in space systems.

© 2005 Elsevier Ltd. All rights reserved.

1. Introduction

1.1. Rationale for implementation of flow boiling in space systems

Boiling heat transfer in microgravity has been the subject of intense study spanning about five decades. However, most of the published literature in this area concerns pool boiling. The absence of a body force in microgravity pool boiling allows bubbles to maintain

contact with the heated wall for an appreciable duration and assume unprecedented bubble size, often approaching that of the heated wall itself [1]. A key drawback to this enormous bubble growth is the difficulty of liquid replenishment of the near-wall region, which can result in very small critical heat flux (CHF) values. Difficulty of containing and maintaining pool boiling in microgravity, coupled with low CHF, are key reasons behind the present-day reluctance to incorporate pool boiling in thermal management hardware for space and planetary-based systems.

Flow boiling is an effective means to overcoming these problems. Bubble detachment in flow boiling is driven largely by liquid inertia, which helps remove bubbles from the heated wall before they coalesce into large,

* Corresponding author. Tel.: +1 765 494 5705; fax: +1 765 494 0539.

E-mail address: mudawar@ecn.purdue.edu (I. Mudawar).

Nomenclature

b	ratio of wetting front length to wavelength
c_h	specific heat of heated wall
c_{pf}	specific heat of liquid
g_e	earth gravity
g_n	gravitational acceleration perpendicular to heated wall
H	channel height
h_{fg}	latent heat of vaporization
k_h	conductivity of heated wall
P	pressure
q''	wall heat flux
q''_m	critical heat flux
$q''_{m,asy}$	asymptotic critical heat flux
q''_w	wetting front lift-off heat flux
T	temperature
$\Delta T_{sub,i}$	inlet subcooling, $T_{sat,in} - T_{in}$
$\Delta T_{sub,o}$	calculated outlet subcooling, $T_{sat,o} - T_o$
U	mean liquid velocity at inlet to heated section of channel
U_f	liquid phase velocity
U_g	vapor phase velocity
z	streamwise coordinate
z^*	extent of continuous upstream wetting region
z_0	streamwise distance where $U_f = U_g$

Greek symbols

δ	mean vapor layer thickness; vapor layer amplitude used in CHF model
δ_h	thickness of heated wall
λ	vapor wavelength
λ_c	critical wavelength
ρ_f	density of saturated liquid
ρ''_f	modified liquid density
ρ_g	density of saturated vapor
ρ''_g	modified vapour density
ρ_h	density of heated wall
σ	surface tension

Subscripts

asy	asymptotic
f	saturated liquid
g	saturated vapor
h	heated wall
in	inlet to heated section of channel
m	maximum, critical heat flux
o	outlet of heated section of channel
sat	saturation
w	heated wall

thermally insulating vapor masses. Furthermore, small bubble size facilitates easier access of bulk liquid to the near-wall region for replenishment. Those two effects result in much greater values for the convective heat transfer coefficient and CHF with flow boiling in microgravity than with pool boiling, especially where the bulk liquid is subcooled.

Recent NASA workshops have culminated in critical recommendations concerning the implementation of flow boiling for a variety of power generation and life support systems [2]. These include Rankine cycle power generation, cabin temperature control, space suit temperature regulation, waste management, electronic cooling, and regenerative fuel cells. Those same workshops called for consolidated efforts to amass empirical data and develop a phenomenologically based understanding of flow boiling. Since virtually no design tools are presently available for implementation of flow boiling in microgravity, key emphasis is being placed on gravity-insensitive or “inertia-dominated” operating conditions.

While very high flow velocities can easily negate the effects of body force and greatly enhance convective heat transfer and CHF, low velocities are preferred because of the stringent power budget constraints of space systems. Hence, there is a strong practical interest in deter-

mining the minimum flow velocity that can effectively overcome any body force effects on CHF in microgravity as well as in lunar and Martian environments.

1.2. Research findings on flow boiling in microgravity

As indicated earlier, very few studies have been published on flow boiling in microgravity. Saito et al. [3] examined flow boiling in microgravity in MU-300 parabolic flight experiments with saturated and subcooled water flow in a $25 \times 25 \text{ mm}^2$ transparent channel. They measured the heat transfer coefficient and observed bubble behavior along the surface of an 8 mm rod heater that was concentric with the channel. In microgravity, they observed bubbles sliding along the heater rod without detachment and coalescing into larger bubbles; detachment was present in earth gravity experiments. The difference in vapor behavior between earth gravity and microgravity was more pronounced at lower velocities, higher heat fluxes and lower liquid subcoolings. However, gravity had little effect on the local heat transfer coefficient along the rod surface. Cochran's studies [4] confirmed the observation that bubbles in microgravity slide along the heated wall and coalesce into larger vapor masses rather than detach into the bulk flow.

Ma and Chung [5,6] examined flow boiling of FC-72 at speeds of 0–0.3 m/s along a $2.54 \times 2.54 \text{ cm}^2$ gold-film heated wall in a 1 s drop tower. They observed that bubble size decreased monotonically with increasing velocity. They suggested that high velocities could negate the effects of gravity on bubble nucleation, growth and departure.

Ohta [7] showed the heat transfer coefficient in annular flow with moderate quality was enhanced by 25% at $2g_e$ compared to earth gravity and deteriorated by 7% in microgravity. Gravity effects disappeared altogether at high velocities, high quality annular flow, and very low quality flow where heat transfer is dominated by nucleate boiling.

Flow boiling CHF data in microgravity are especially rare. Ma and Chung [8] attempted to obtain microgravity CHF data by flowing FC-72 across a 0.254 mm diameter heated platinum wire in a 2.1 s drop tower. They generated boiling curves extending from the single-phase region to CHF for flow velocities of 0.078, 0.22 and 0.3 m/s. For the same velocity, CHF was lower in microgravity than in earth gravity, but those differences decreased with increasing velocity. They suggested gravity effects should disappear altogether at sufficiently high velocities.

Clearly, more work needs to be done to quantify these important observations in pursuit of a fundamental understanding of the underlying microgravity effects and the relationship between CHF and flow velocity at both microgravity and earth gravity. The present study aims to (1) amass new microgravity flow boiling CHF data, (2) compare those data to CHF in earth gravity, (3) present a systematic theoretical scheme to determine the effects of body force on CHF, and (4) determine the minimum flow velocity that would yield appreciable diminution in the effects of gravity on CHF.

2. Experimental methods

2.1. Flow boiling module

A flow boiling module was formed by bolting together two transparent polycarbonate plastic (Lexan) plates between two aluminum support plates. As shown in Fig. 1(a), the flow channel was constructed by milling a $5.0 \times 2.5 \text{ mm}^2$ rectangular slot into the underside of the top plate. The bottom plate was hollowed in the middle to support a 0.56 mm thick oxygen-free copper plate to the underside of which resistive heaters were soldered. The copper plate was held firmly in place when the two channel plastic plates were clamped together. A leak-proof seal was maintained by a flexible Teflon cord that was inserted into a shallow O-ring groove in the upper surface of the bottom Lexan plate. A honeycomb insert was placed at the channel inlet to straighten the

flow and break up any large eddies. An entry length 106 times the channel hydraulic diameter provided a hydrodynamically fully developed flow upstream of the copper plate (heated portion of the channel). Just upstream and downstream of the copper plate, thermocouples were inserted into the middle of the channel to measure fluid temperature, while pressure taps in the bottom plate measured static pressure at those two locations.

2.2. Heated wall design and thermal response

The channel heater was carefully optimized to provide fast temperature response during parabolic flight experiments. As shown in Fig. 1(b), the heater consisted of the 0.56 mm thick copper plate to which a series of six thick-film resistors were soldered. Each resistor measured $16.1 \times 4.0 \text{ mm}^2$ and had a resistance of about 188 Ω . Five thermocouples were inserted into shallow holes in the copper plate between the resistors, aligned along the centerline of the plate. The six resistors were connected in a parallel electrical circuit. To preclude any variations in power dissipation, the six resistors were carefully selected from a large batch of resistors based on equal resistance values. This ensured equal current draw through each resistor and a uniform heat flux along the copper surface. Power to the resistors was supplied from a variable voltage transformer. The power input was determined from current and voltage measurements.

As indicated earlier, the thickness of the copper plate was carefully selected to provide fast temperature response during the parabolic flight experiments. But while fast response favors a very small thickness, special effort was made to preclude any CHF dependence on copper plate thickness. This latter concern is crucial to obtaining useful CHF data representative of real engineering surfaces. Previous studies have shown that the thickness, δ_h , and thermal properties (k_h, ρ_h, c_h) of the heating wall can have a measurable influence on CHF [9,10]. Using saturated pool boiling CHF data for FC-72, Golobic and Bergles [11] correlated these effects according to

$$\frac{q''_m}{q''_{m,asy}} = 1 - e^{-\left(\frac{\delta_h \sqrt{\rho_h c_h k_h}}{2.44}\right)^{0.8498} - \left(\frac{\delta_h \sqrt{\rho_h c_h k_h}}{2.44}\right)^{0.0581}}, \quad (1)$$

where $q''_{m,asy}$ is called the asymptotic CHF. Fig. 2(a) shows the variation of CHF for FC-72 with copper wall thickness according to Eq. (1). Notice that very thin walls produce fairly small CHF values and CHF increases with increasing thickness up to 0.4 mm, above which it is equal to the asymptotic value. Most copper and other metallic walls of practical interest fall within the asymptotic range. Hence, it is important to employ a wall thickness for CHF measurement that also falls in the asymptotic range, i.e. having $\delta_h > 0.40 \text{ mm}$. Fig.

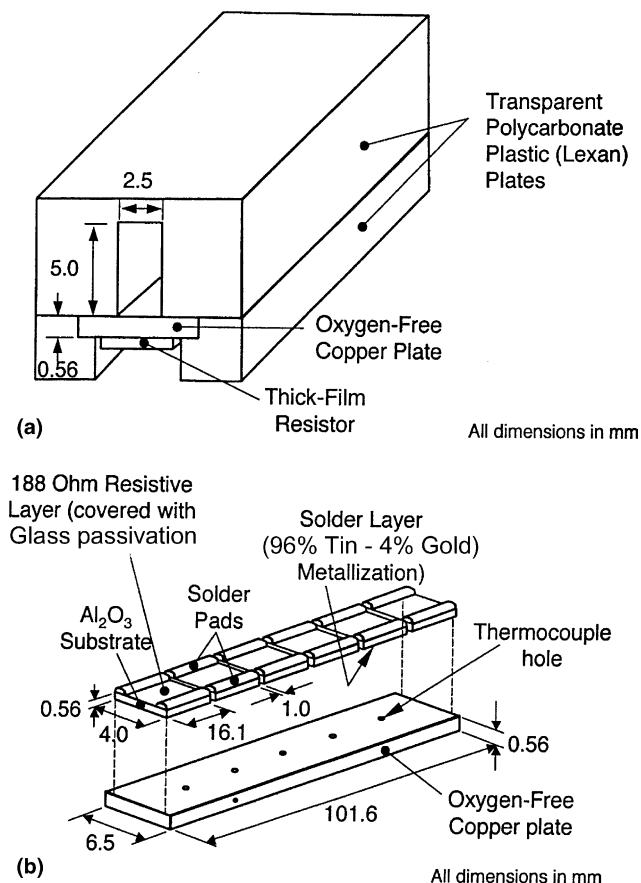


Fig. 1. (a) Flow channel assembly and (b) construction of heated wall.

2(a) proves the thin gold foil heaters often used in microgravity boiling studies measure CHF values far smaller than those of practical surfaces.

To achieve the fastest thermal response during parabolic flight experiments, the copper wall thickness must therefore be maintained as small as possible but satisfy the asymptotic CHF criterion. A thickness of 0.56 mm was deemed effective at satisfying both criteria. Fig. 2(b) shows the wall temperature in the present wall design reached steady state in less than 5 s following a heat flux increment, which is well within the 23 s duration of microgravity in a single parabolic maneuver. Fig. 2(c) shows the wall temperature response during the parabola.

2.3. Fluid conditioning loop

Fluid conditioning was accomplished with the aid of a compact two-phase flow loop illustrated schematically in Fig. 3(a). The loop consisted of a reservoir, magnetically coupled centrifugal pump, flow control valve, filter, flowmeter, in-line heater, flow boiling module, heat exchanger, and accumulator. Four immersion heaters in

the reservoir were used to boil the liquid for deaeration purposes. The fluid reservoir was disconnected from the loop prior to boarding the jet. The accumulator served as a thermal expansion compensator and pulsation dampener to ensure flow stability and maintain the desired pressure downstream from the test section. The liquid flow rate was modulated by the flow control valve and measured by a turbine flowmeter. The fluid temperature was regulated by the liquid-to-air heat exchanger and fine-tuned with the aid of the in-line electric heater. A variable transformer controlled the fan speed of the heat exchanger.

The entire test facility, including the flow loop components, power and instrumentation cabinets, and data acquisition system, was mounted onto a rigid extruded aluminum frame depicted in Fig. 3(b). The frame was fastened to the floor of the jet.

2.4. Photographic techniques

An NAC HSV-500 high-speed video system was used to record vapor-liquid interfacial features along the heated wall. The video camera in this system features a

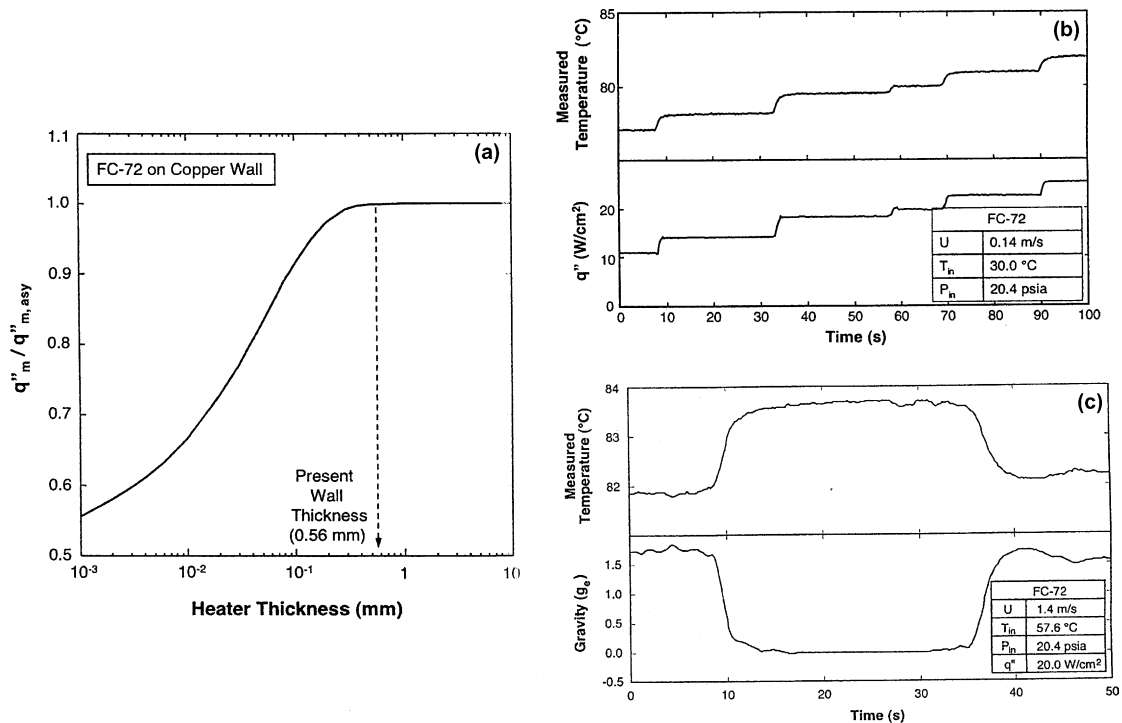


Fig. 2. (a) Effect of wall thickness on CHF and thermal response of heated wall (b) with changing heat flux and (c) during single parabolic maneuver.

recording time of up to 43 min on S-VHS tape. To avoid the effects of intense heating of tungsten light sources on the boiling process, let alone potential hazards to the operator during the flight experiments, a custom light source was devised for this study. It consisted of an array of 240 LEDs, each having a brightness of 14,000 candles. The light source was separated from the channel by light diffusion sheets. The video camera was positioned normal to the side of the flow channel and captured the downstream half of the heated copper wall. Video images were recorded at 250 fps with a shutter speed of 100 μ s. The time interval between consecutive images (presented later) was 8 ms.

2.5. Test procedure

The reduced gravity environment was achieved by flying a NASA KC-135 turbojet through a series of parabolic maneuvers as illustrated in Fig. 4(a). Each parabola was initiated with a 1.8g_e pull-up and terminated with a 1.8g_e pullout. Fig. 4(b) shows the actual acceleration recorded during two parabolas. The microgravity period in a single maneuver lasted about 23 s. A normal mission lasting approximately 2 h consisted of 40 parabolic maneuvers. The flight was usually divided into 4 sets of 10 parabolas with about a 5 min

break between consecutive sets. This study is based on data collected from 8 flight missions or about 320 parabolas.

The desired operating conditions were set before each set of parabolas by regulating the various components of the flow loop. Power was supplied to the copper wall resistors of the flow channel before each parabola and maintained during the parabola. The wall heat was increased by 1–3 W/cm² for each parabola until CHF was detected. Flow conditions, wall temperatures, heated wall power input and acceleration were recorded continuously. Video images were recorded for about 50 s covering the entire microgravity period of each parabola. Aside from microgravity, there was some interest in flow boiling behavior in both lunar and Martian environments. A few parabolic maneuvers were therefore dedicated to those environments.

FC-72 was used as working fluid. The operating conditions for this study were as follows: outlet pressure of $P_o = 138$ – 152 kPa (20–22 psia), outlet subcooling of $\Delta T_{sub,o} = 2$ – 23 °C, and inlet liquid velocity of $U = 0.14$ – 1.5 m/s.

The accuracies of flow rate, pressure, and heat flux measurements were 2.3%, 0.01%, and 0.2%, respectively. The fluid and wall temperatures were measured with thermocouples having an uncertainty of 0.3 °C.

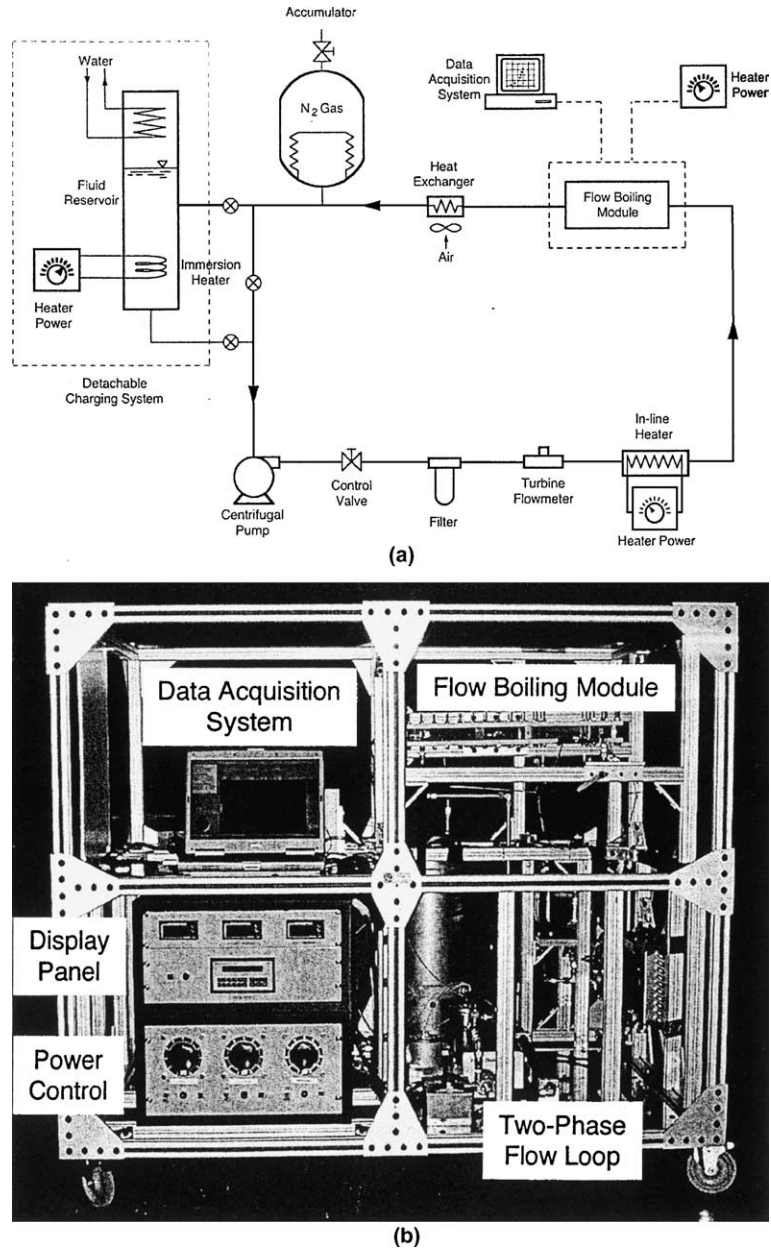


Fig. 3. (a) Schematic of two-phase flow loop and (b) photo of flight apparatus.

3. Gravity effects on flow boiling behavior

As indicated in Fig. 4(a), a parabolic maneuver included a short duration of $1.8g_e$ prior to the 23 s microgravity period. Fig. 5 shows vapor behavior captured during the last of a series of maneuvers for a relatively low velocity of $U = 0.25$ m/s and $\Delta T_{\text{sub},0} = 4.1$ °C. This is the maneuver corresponding to the last heat flux increment that precipitated CHF as the KC-135 entered microgravity. CHF is defined as the last stable condition

prior to a sudden unsteady increase in the wall temperature. Shown are drastic differences in vapor behavior at $1.8g_e$ compared to μg_e . At $1.8g_e$, vapor bubbles were detached from the heated wall and driven across the channel by the strong buoyancy associated with this relatively high gravitational level (g -field is perpendicular to the heated wall shown at the bottom of each image). This boiling behavior is reminiscent of pool boiling at $1g_e$ because of the dominance of buoyancy force perpendicular to the wall compared to the drag forces exerted

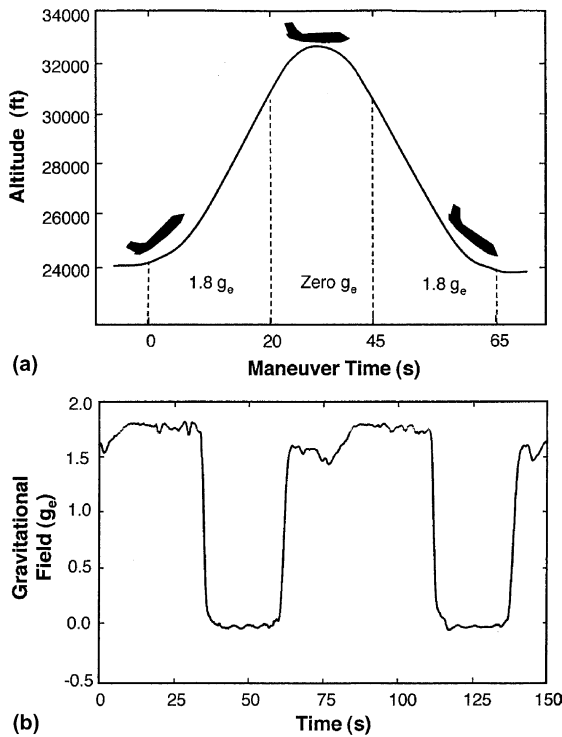


Fig. 4. (a) Trajectory and (b) gravity change of parabolic flight.

on the bubbles in a direction parallel to the wall. Microgravity negates any buoyancy effects perpendicular to the wall, causing bubbles to remain attached to the wall,

grow as they slide slowly along, and coalesce into large vapor patches.

Fig. 6 shows sequential images of flow boiling at a very low velocity of $U = 0.14 \text{ m/s}$ and $\Delta T_{\text{sub,o}} = 22.8 \text{ }^\circ\text{C}$ for $1.8g_e$, $0.17g_e$ (lunar gravity) and μg_e . These conditions correspond to the same heat flux of 17.1 W/cm^2 that precipitated CHF in μg_e . Appreciable differences are evident, with the $1.8g_e$ yielding strong detachment from the wall, $0.17g_e$ producing minimal detachment and greater coalescence, and μg_e producing no detachment and appreciable coalescence and vapor patch growth. It is important to note that condensation played a more important role for these cases compared to those depicted in Fig. 5, where $\Delta T_{\text{sub,o}} = 4.1 \text{ }^\circ\text{C}$. Bubbles at $1.8g_e$ and $\Delta T_{\text{sub,o}} = 22.8 \text{ }^\circ\text{C}$ appeared to condense more rapidly and shrink in size as they detached from the wall and traveled across the flow channel. The same high subcooling affected vapor production at μg_e , Fig. 6(c), albeit in a different manner. Here, bulk subcooling condensed vapor along the top interface of the vapor patches as well as between patches.

Higher liquid velocities greatly dampened the effects of gravity. Fig. 7 shows sequential images captured at a relatively high velocity of $U = 1.4 \text{ m/s}$ and $\Delta T_{\text{sub,o}} = 5.6 \text{ }^\circ\text{C}$ for $1.8g_e$, $0.377g_e$ (Martian gravity), and μg_e as well. Heat flux for all three cases is equal to the heat flux that triggered CHF in μg_e . At $1.8g_e$, some vapor detachment from the wall did occur, but the detached bubbles could hardly reach the opposite wall due to the strong drag force exerted by the liquid. This resulted in significant pileup of vapor along the heated wall as well as coalescence into larger vapor patches.

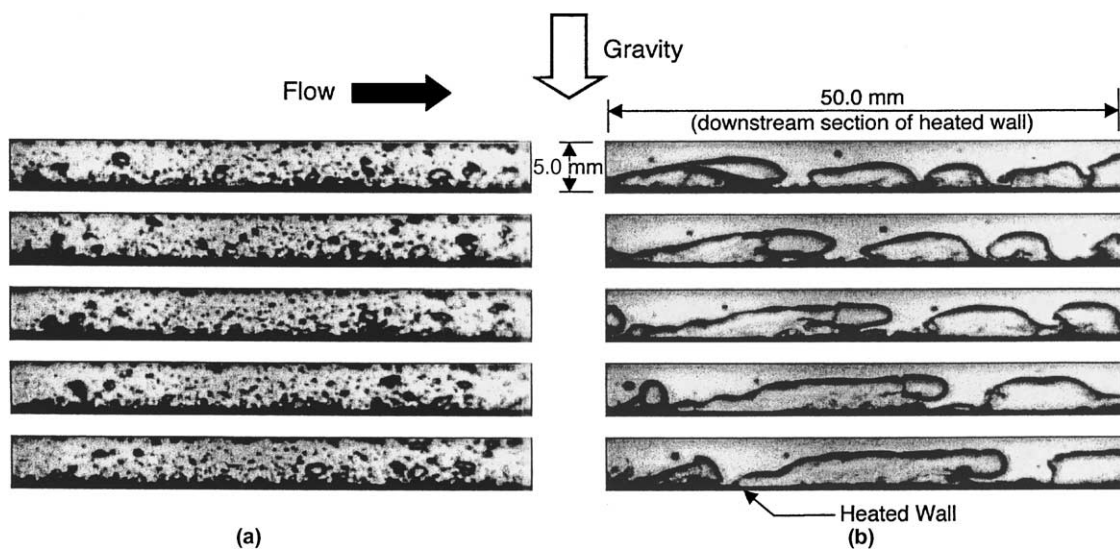


Fig. 5. Sequential images for $U = 0.25 \text{ m/s}$, $\Delta T_{\text{sub,o}} = 4.1 \text{ }^\circ\text{C}$ and $q'' = 15.4 \text{ W/cm}^2$ (corresponding to CHF at μg_e) for (a) $1.8g_e$ and (b) μg_e .

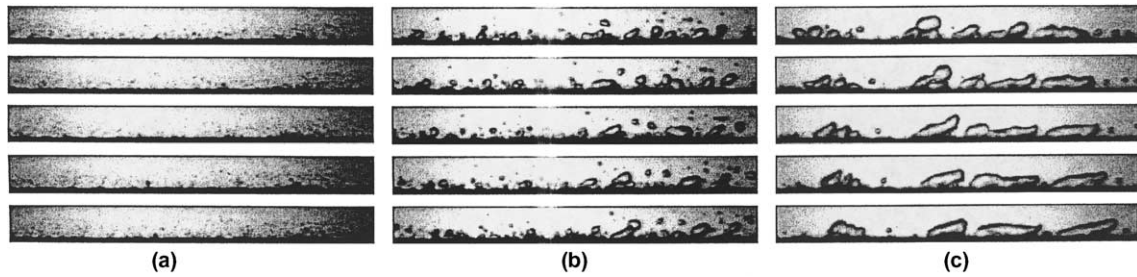


Fig. 6. Sequential images for $U = 0.14$ m/s, $\Delta T_{\text{sub,o}} = 22.8$ °C and $q'' = 17.1$ W/cm² (corresponding to CHF at μg_e) for (a) $1.8g_e$, (b) Lunar- g ($0.17g_e$) and (c) μg_e .

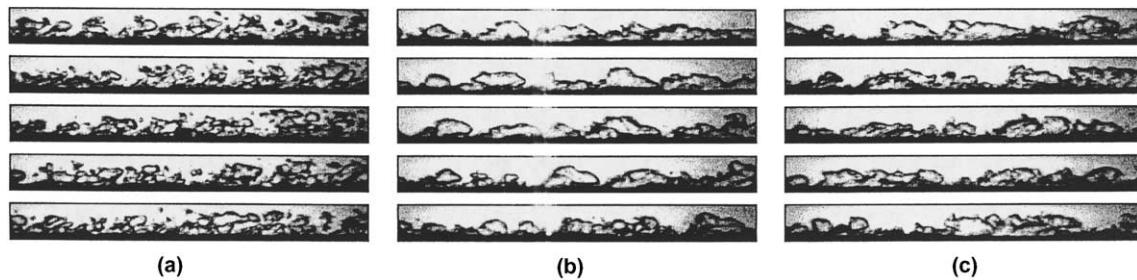


Fig. 7. Sequential images for $U = 1.4$ m/s, $\Delta T_{\text{sub,o}} = 5.6$ °C and $q'' = 28.4$ W/cm² (corresponding to CHF at μg_e) for (a) $1.8g_e$, (b) Martian- g ($0.377g_e$) and (c) μg_e .

At $0.377g_e$ and μg_e , detachment was nonexistent and all the vapor was amassed into large vapor patches. There were hardly any discernible differences in boiling behavior between those two cases.

4. CHF mechanism in microgravity

A key objective of the present study is to develop a fundamental understanding of the flow boiling CHF mechanism in microgravity. This was accomplished by recording interfacial activity along the heated wall with increasing heat flux up to and including CHF.

Fig. 8 shows for $U = 0.15$ m/s and $\Delta T_{\text{sub,o}} = 3.0$ °C the boiling curve and corresponding interfacial behavior with increasing heat flux in μg_e . Without a buoyancy force perpendicular to the heated wall, vapor masses simply slid axially along the wall. For 63% and 73% of CHF in μg_e , small bubbles can be observed coalescing into larger ones along the wall. Coalescent bubble size increased noticeably at 81%. At 91% CHF in μg_e , most of the vapor was amassed into fairly long vapor patches that propagated along the heated wall. Just prior to CHF, the patches increased appreciably in size, precluding liquid access to the wall save for small troughs—wetting fronts—between the vapor patches. Eventually, the liquid–vapor interface began to separate from the wall

by the intense momentum of vapor generated in the troughs.

To better identify the trigger mechanism for CHF in microgravity, the interfacial behavior was recorded during the CHF transient. Fig. 9 depicts sequential images recorded in μg_e just before, during, and just after CHF for $U = 0.15$ m/s and $\Delta T_{\text{sub,o}} = 3.0$ °C. At CHF-, a series of very long vapor patches propagated along the wall. Despite some boiling activity in a liquid sublayer beneath the vapor patches, much of the wall energy appeared to be released to liquid in the wetting fronts between the vapor patches. The sublayer boiling activity subsided altogether during the CHF transient as only the troughs were able to sustain cooling for the wall. Notice in Fig. 9(b) that the vapor patches constitute a fairly continuous vapor layer. The downstream wetting front appears to maintain partial contact with the wall. This is the moment when the wall temperature began increasing in an unsteady manner as fewer wetting fronts were available for cooling. Fig. 9(c) shows two wetting fronts lifting off the wall as virtually all liquid access was lost. This is where the wall temperature began to escalate at a fast rate as film boiling ensued.

Fig. 10 depicts the CHF transient in μg_e for $U = 1.5$ m/s and $\Delta T_{\text{sub,o}} = 3.8$ °C. Vapor patches appear to propagate along the wall in this case as well, separated by liquid wetting fronts. The patches are far shorter and

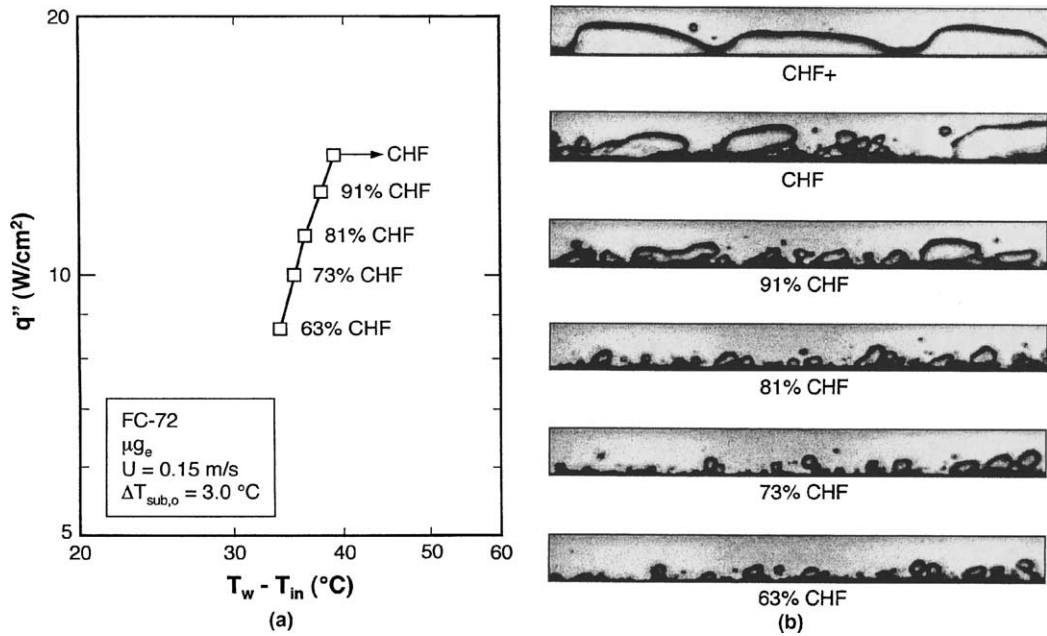


Fig. 8. (a) Boiling curve and (b) vapor behavior at different heat fluxes in μg_e for $U = 0.15$ m/s and $\Delta T_{sub,0} = 3.0$ °C.

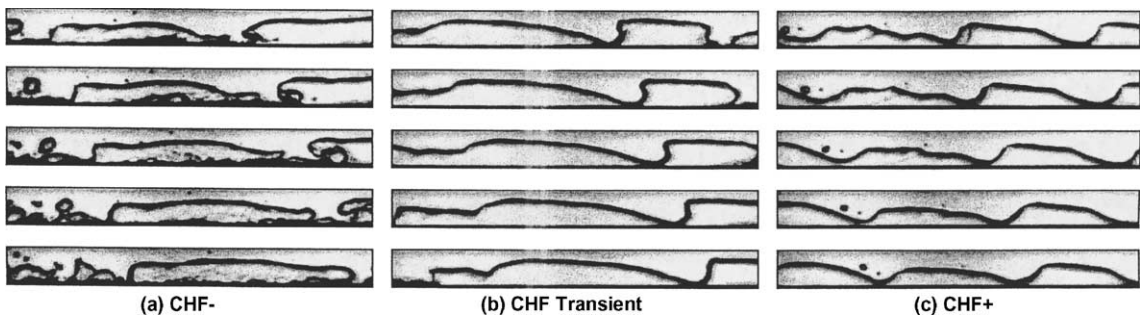


Fig. 9. CHF transient in μg_e for $U = 0.15$ m/s and $\Delta T_{sub,0} = 3.0$ °C.

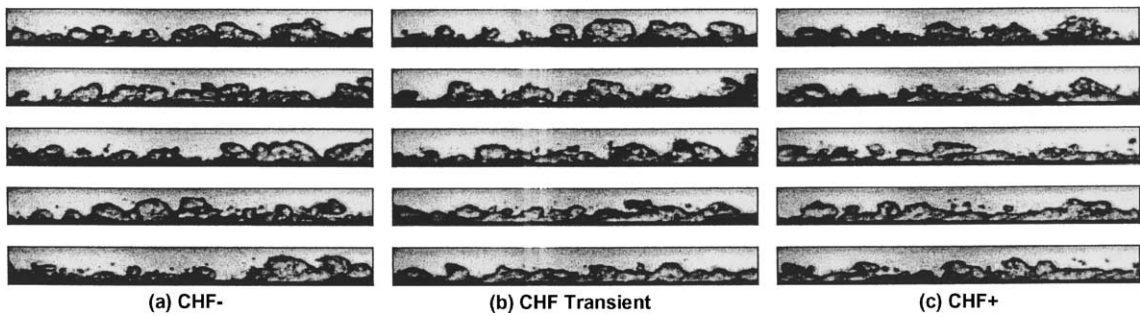


Fig. 10. CHF transient in μg_e for $U = 1.50$ m/s and $\Delta T_{sub,0} = 3.8$ °C.

their interface significantly more perturbed than at 0.15 m/s. These made the depiction of vapor activity in the wetting fronts a bit elusive.

The interfacial behavior depicted in Figs. 9 and 10 follows very closely earlier CHF depictions by Galloway and Mudawar [12,13] for vertical upflow along a short

heated wall. Those earlier depictions formed a mechanistic foundation for the development of the Interfacial Lift-off CHF Model, which showed excellent accuracy in predicting data by Galloway and Mudawar and later by Sturgis and Mudawar [14,15].

As a prelude to the present study, Zhang et al. [16–19] explored the effects of body force on CHF in earth gravity by examining flow boiling in a channel that was tilted at different orientations. Six CHF regimes were identified. The first and most dominant is the *Wavy Vapor Layer regime* that followed very precisely Galloway and Mudawar's Interfacial Lift-off Model. This regime included all vertical upflow conditions as well as channel orientations corresponding to relatively high flow velocities. These are conditions with either no component of body force perpendicular to the wall, or where body force effects are insignificant compared to liquid inertia. Interesting, all five other CHF regimes that were identified by Zhang et al. were associated with low velocities, downflow, or downward-facing heated wall orientations for which the body force perpendicular to the heated wall was important.

When comparing the present μg_e experiments with those of Zhang et al., it appears that in μg_e (1) the five body-force-sensitive CHF regimes are nonexistent, and (2) the Wavy Vapor regime is prevalent at *all* flow velocities.

5. CHF results

The Interfacial Lift-off Model used to describe CHF in the Wavy Vapor Layer regime is based upon a vapor-layer interfacial instability dominated by a balance between surface tension, inertia, and body force. This instability is responsible for the advantageous liquid contact with the wall in the wetting fronts of the vapor layer. This contact is maintained by a pressure force exerted upon the interface due to interfacial curvature as shown in Fig. 11. The Interfacial Lift-off Model is based on the hypothesis that the interface will separate from the wall in the wetting fronts when the momentum of the vapor produced in the wetting fronts perpendicular to the wall just exceeds the interfacial pressure force [12,13].

To explore the effectiveness of the Interfacial Lift-off Model, flow boiling CHF data were obtained in μg_e aboard NASA's KC-135 turbojet and then repeated on ground (at $1g_e$) in a horizontal orientation. Fig. 12 shows the variation of CHF with velocity at $1g_e$ and μg_e . In μg_e , CHF increases appreciably with increasing velocity. However, the flow velocity has a far smaller effect at $1g_e$. At the lowest velocity, CHF at μg_e is only 50% of that at $1g_e$. Increasing velocity helps to reduce the difference between the two gravitational environments, with the CHF data converging around 1.5 m/s.

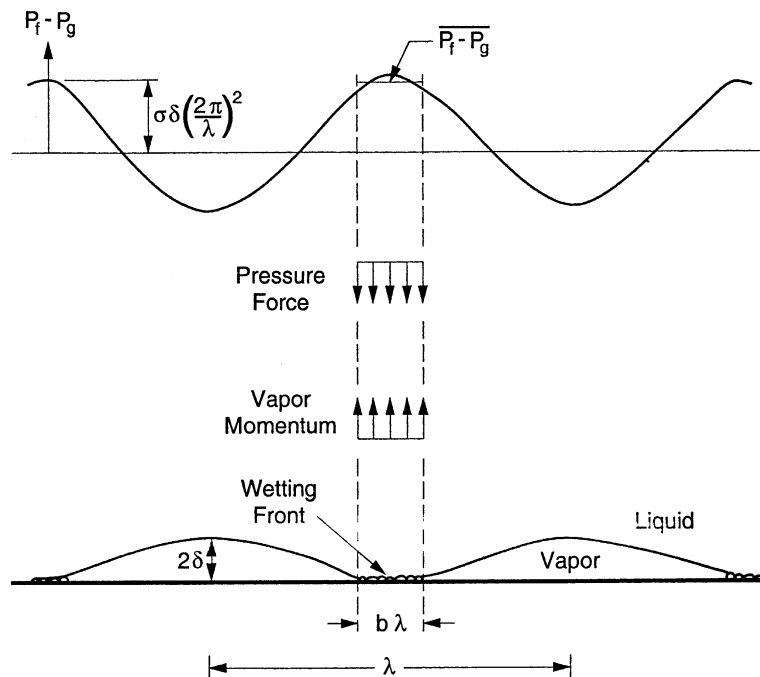


Fig. 11. Balance of vapor momentum and interfacial pressure difference at moment of wetting front separation according to Interfacial Lift-off Model [17].

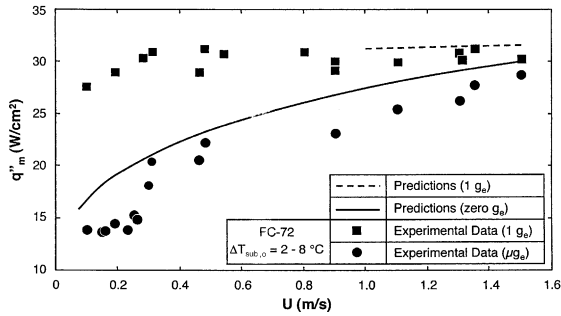


Fig. 12. Comparison of CHF data and Interfacial Lift-off Model predictions for μg_e and horizontal $1g_e$ flow boiling.

Also included in Fig. 12 are CHF predictions based on the Interfacial Lift-off Model. Details of this model were recently provided by Zhang et al. [17] for the Wavy Vapor Layer CHF regime. The model consists of sub-models for interfacial instability, mass, momentum and energy conservation, and an interfacial lift-off criterion. A summary of the model’s key equations is given in Table 1. Notice in Fig. 12 that the Interfacial Lift-off Model provides predictions for μg_e over the entire velocity range, while only high velocity predictions are possible for $1g_e$ since horizontal flow at $1g_e$ at lower

velocities is associated with the “Pool Boiling” CHF regime [17], which is fundamentally different from the Wavy Vapor Layer regime.

The CHF predictions point out very important facts that are of great significance to space missions. First, these predictions prove that, unlike in $1g_e$, CHF in μg_e is dominated by the Wavy Vapor Layer regime regardless how small is the flow velocity. Second, it shows CHF for μg_e can be accurately predicted by the Interfacial Lift-off Model. Third, the convergence of μg_e and $1g_e$ data at about 1.5 m/s proves it is possible to design inertia-dominated space systems by maintaining flow velocities above this convergence limit. Inertia-dominated systems allow data, correlations, and/or models developed at $1g_e$ to be safely implemented in space systems.

It is important to emphasize that the convergence limit is both fluid and geometry dependent, but can be easily predicted by the Interfacial Lift-off Model. A more thorough treatment of the convergence limit is available in Ref. [19].

6. Conclusions

This study investigated flow boiling CHF in microgravity that was achieved in parabolic flight experiments. Other gravitational environments (high- g_e , Martian, lunar) were also tested in to better understand the effects of body force on CHF. The microgravity experiments were later repeated in horizontal $1g_e$ ground experiments to explore key differences in vapor behavior between the two environments. High-speed video imaging played a key role in all these experiments by provided sequential records of vapor layer development during nucleate flow boiling up to and including the CHF transient. Key findings from this study are as follows:

- (1) With an acceleration of $1.8g_e$ perpendicular to the heated wall, bubbles in low velocity flow are detached and driven across the flow channel resembling behavior observed in pool boiling at $1g_e$. The detachment precludes bubble coalescence along the heated wall and greatly reduces bubble size, especially in highly subcooled flow.
- (2) No bubble detachment is observed in microgravity where bubbles quickly coalesce to fairly large vapor patches that slide along the heated wall. This behavior is prevalent for all flow velocities.
- (3) As CHF is approached in microgravity, the vapor patches grow in length and take the form of a wavy vapor layer that propagates along the wall, permitting liquid access to the wall only in the wave troughs—wetting fronts. CHF is triggered by separation of the liquid–vapor interface from the wall due to intense vapor effusion in the

Table 1

Key equations of interfacial lift-off model

Phase velocities:

$$U_g = \frac{q''_m z}{\rho_g \delta (c_{p,f} \Delta T_{sub,i} + h_{fg})}$$

$$U_g = \frac{UH}{H - \delta} - \frac{q''_m z}{\rho_f (H - \delta) (c_{p,f} \Delta T_{sub,i} + h_{fg})}$$

Critical wavelength:

$$\frac{2\pi}{\lambda_c} = \frac{\rho''_f \rho''_g (U_g - U_f)^2}{2\sigma(\rho''_f + \rho''_g)} + \sqrt{\left[\frac{\rho''_f \rho''_g (U_g - U_f)^2}{2\sigma(\rho''_f + \rho''_g)} \right]^2 + \frac{(\rho_f - \rho_g) g_n}{\sigma}}$$

where $\rho''_f = \rho_f \coth\left[\frac{2\pi}{\lambda_c}(H - \delta)\right]$ and $\rho''_g = \rho_g \coth\left(\frac{2\pi}{\lambda_c} \delta\right)$

Average interfacial pressure difference for wetting front:

$$\overline{P_f} - \overline{P_g} = \frac{4\pi\sigma\delta \sin(b\pi)}{\lambda_c^2 b}$$

where $b = 0.20$

Interfacial lift-off heat flux in wetting front:

$$q''_w = \rho_g (c_{p,f} \Delta T_{sub,i} + h_{fg}) \left(\frac{\overline{P_f} - \overline{P_g}}{\rho_g} \right)^{1/2}$$

Heated wall energy balance:

$$q''_m = b q''_w$$

Critical heat flux:

$$q''_m = \rho_g (c_{p,f} \Delta T_{sub,i} + h_{fg}) \left[\frac{4b\pi\sigma \sin(b\pi)}{\rho_g} \right]^{1/2} \frac{\delta^{1/2}}{\lambda_c^{1/2} z^*}$$

where $z^* = z_0 + \lambda_c(z^*)$ and z_0 is the stream-wise distance from leading edge of heated wall where $U_f = U_g$

wetting fronts. This behavior is consistent with, and accurately predicted by the Interfacial Lift-off CHF Model.

- (4) CHF in microgravity at low velocities is significantly smaller than in horizontal flow at $1g_e$. The difference in CHF magnitude between the two environments decreases with increasing velocity, culminating in a virtual convergence of μg_e and $1g_e$ data at 1.5 m/s for FC-72. This proves it is possible to design inertia-dominated space systems by maintaining flow velocities above the convergence limit. Such inertia-dominated systems allow data, correlations, and/or models developed at $1g_e$ to be safely implemented in space systems.

Acknowledgements

The authors are grateful for the support of the National Aeronautics and Space Administration under Grant no. NNC04GA54G. Several individuals provided valuable assistance in preparing the apparatus for the flight experiments and obtaining flight data. The authors thank John Sankovic, John McQuillen, Glenda Yee, Dr. Juan Agui and Dr. Charles Niederhaus of the NASA Glenn Center, Arthur Stachowicz and William Birchenough of ZIN Technologies Inc., and Dwayne Kiefer, Elizabeth Gray and Robert Skupinski of QSS Group Inc. for their assistance.

References

- [1] J. Kim, J.F. Benton, Subcooled pool boiling heat transfer in earth gravity and microgravity, in: Proc. 2001 National Heat Transfer Conference, Anaheim, CA, 2001.
- [2] F.P. Chiamonte, J.A. Joshi, Workshop on critical issues in microgravity fluids, transport, and reaction processes in advanced human support technology—Final report, NASA TM-2004-212940, 2004.
- [3] M. Saito, N. Yamaoka, K. Miyazaki, M. Kinoshita, Y. Abe, Boiling two-phase flow under microgravity, Nucl. Eng. Des. 146 (1994) 451–461.
- [4] T.H. Cochran, Forced-convection boiling near inception in zero-gravity, NASA TN D-5612, 1970.
- [5] Y. Ma, J.N. Chung, An experimental study of forced convection boiling in microgravity, Int. J. Heat Mass Transfer 41 (1998) 2371–2382.
- [6] Y. Ma, J.N. Chung, A study of bubble dynamics in reduced gravity forced-convection boiling, Int. J. Heat Mass Transfer 44 (2001) 399–415.
- [7] H. Ohta, Experiments on microgravity boiling heat transfer by using transparent heaters, Nucl. Eng. Des. 175 (1997) 167–180.
- [8] Y. Ma, J.N. Chung, An experimental study of critical heat flux (CHF) in microgravity forced-convection boiling, Int. J. Multiphase Flow 27 (2001) 1753–1767.
- [9] R. Cole, H.L. Shulman, Critical heat flux at sub-atmospheric pressures, Chem. Eng. Sci. 21 (1966) 723–724.
- [10] G. Guglielmini, E. Nannei, On the effect of heating wall thickness on pool boiling burnout, Int. J. Heat Mass Transfer 19 (1976) 1073–1075.
- [11] I. Golobic, A.E. Bergles, Effects of heater side factors on the saturated pool boiling critical heat flux, Exp. Thermal Fluid Sci. 5 (1997) 43–51.
- [12] J.E. Galloway, I. Mudawar, CHF mechanism in flow boiling from a short heated wall—Part 1. Examination of near-wall conditions with the aid of photomicrography and highspeed video imaging, Int. J. Heat Mass Transfer 36 (1993) 2511–2526.
- [13] J.E. Galloway, I. Mudawar, CHF mechanism in flow boiling from a short heated wall—Part 2. Theoretical CHF model, Int. J. Heat Mass Transfer 36 (1993) 2527–2540.
- [14] J.C. Sturgis, I. Mudawar, Critical heat flux in a long, rectangular channel subjected to one-sided heating—I. Flow visualization, Int. J. Heat Mass Transfer 42 (1999) 1835–1847.
- [15] J.C. Sturgis, I. Mudawar, Critical heat flux in a long, rectangular channel subjected to one-sided heating—II. Analysis of critical heat flux data, Int. J. Heat Mass Transfer 42 (1999) 1849–1862.
- [16] H. Zhang, I. Mudawar, M.M. Hasan, Experimental assessment of the effects of body force, surface tension force, and inertia on flow boiling CHF, Int. J. Heat Mass Transfer 45 (2002) 4079–4095.
- [17] H. Zhang, I. Mudawar, M.M. Hasan, Experimental and theoretical study of orientation effects on flow boiling CHF, Int. J. Heat Mass Transfer 45 (2002) 4463–4478.
- [18] H. Zhang, I. Mudawar, M.M. Hasan, Investigation of interfacial behavior during the flow boiling CHF transient, Int. J. Heat Mass Transfer 47 (2004) 1275–1288.
- [19] H. Zhang, I. Mudawar, M.M. Hasan, A method for assessing the importance of body force on flow boiling CHF, ASME J. Heat Transfer 126 (2004) 161–168.